Supplementary Information:

Exploring the effect of pressure on the crystal structure and caloric properties of the molecular ionic hybrid $[(CH_3)_3NOH]_2[CoCl_4]$

Pedro Dafonte-Rodriguez[a,†], Ignacio Delgado-Ferreiro[a,†], Javier García-Ben, Angel Ferradanes-Martínez[a], María Gelpi[a], Julian Walker[b], Charles James McMonagle[c], Socorro Castro-García[a], María Antonia Señarís-Rodríguez[a], Juan Manuel Bermúdez-García[a,] and Manuel Sánchez-Andújar[a,**]*

[a] *University of A Coruna, QUIMOLMAT Group, Dpt. Chemistry, Faculty of Science and Centro Interdisciplinar de Química e Bioloxía (CICA), Zapateira, 15071 A Coruña, Spain*.

*j.bermudez@udc.es, **m.andujar@udc.es

[b] *Norwegian University of Science and Technology, Department of Materials Science and Engineering, Trondheim 7491, Norway.*

[c] *European Synchrotron Radiation Facility, Swiss-Norwegian Beamlines, Grenoble 3843, France.*

[†] *These authors have equally contributed to this work*

Synthetic method

Starting materials: *C*ommercially available $(CH_3)_3NO{\cdot}2H_2O$ (98%, Acros Organics), HCl solution (ca. 37% in H_2O, Fischer Chemical), $CoCl_2{\cdot}6H_2O$ (98%, Aldrich) and CH_3OH (pure, Fischer Chemical) were used as starting materials without further purification.

The synthesis procedure was similar to that previously reported for $[(CH_3)_3NOH]_2ZnCl_4$ *(X.M. Chen et al., Chem. Commun., 2019,* ***55****, 8983)* with a slight modification on the employed solvent. For comparison purposes, we have also synthesized this reported $[(CH_3)_3NOH]_2[ZnCl_4]$ compound following the literature.

Synthesis of N-hydroxyl ammonium chloride: The salt $[(CH_3)_3NOH]Cl$ was synthesized via neutralization of an aqueous solution of $(CH_3)_3NO{\cdot}2H_2O$ with an excess of HCl 37% p/p. For this purpose, the acid solution was added drop by drop to the aqueous solution of $(CH_3)_3NO$ and this latter was cooled using an ice-water bath. The mixture was concentrated to dryness using a rotary evaporator until obtain a white polycrystalline powder.

Synthesis of $[(CH_3)_3NOH]_2[CoCl_4]$: Previously synthetized $[(CH_3)_3NOH]Cl$ and commercial $CoCl_2{\cdot}6H_2O$ were used to obtain $[(CH_3)_3NOH]_2[CoCl_4]$ as it follow: stoichiometric amounts of $[(CH_3)_3NOH]Cl$ and $CoCl_2{\cdot}6H_2O$ were dissolved in separated CH_3OH solutions, and after that, both were mixed. A dark blue polycrystalline powder of $[(CH_3)_3NOH]_2[CoCl_4]$ was obtained upon slow evaporation of the solvent at room temperature after several days and the obtained powder was isolated by filtration and washed several times with diethyl ether.

Experimental section

Powder X-ray diffraction and Synchrotron Radiation Powder X-ray diffraction

Powder X-ray diffraction (PXRD) patterns of the obtained polycrystalline powders were collected in a Siemens D-5000 diffractometer using CuK_α radiation at room temperature.

Synchrotron powder X-ray diffraction (SPXRD) patterns of $[(CH_3)_3NOH]_2[CoCl_4]$ was recorded at the BM01 beamline of the ESRF Synchrotron (Grenoble, France) using a wavelength of 0.71073 Å at room temperature. The wavelength was determined by refining the positions of six individual reflections of a NIST660 LaB_6 standard collected with a Pilatus 2M detector. The recorded 2D patterns were integrated into a 1D powder profile. For this purpose, the sample was enclosed in a glass capillary (inner diameter ϕ = 0.5 mm) and in continuous rotation during data collection to improve powder averaging. The pressure cell system was designed and manufactured by Dr. Charles J. McMonagle, it consists of a high-pressure hydraulic pump to generate the pressure and a sapphire capillary cell that contains the sample to be investigated. The pressure cell is made from a 100 mm long, open-at-both-ends, sapphire capillary (α-Al2O3, provided by CRYTUR) with an outer diameter of 2 mm and an inner diameter of 0.6 mm (reported in C. J. McMonagle, *et al.*, *J. Appl. Crystallogr.*, 2020, **53**, 1519–1523). LeBail refinement was carried out using the program GSAS-II.

Single crystal X-ray diffraction

Single-crystal X-ray diffraction (SCXRD) experiments were carried out at 100 K, 150 K and room temperature. For that purpose, single-crystal diffraction data sets of one crystal were collected at room temperature in a Bruker D8 VENTURE Kappa X-ray diffractometer equipped with a PHOTON III detector and using monochromatic MoKα radiation (λ=0.71073 Å).

A suitable crystal was chosen and mounted on a MiTeGen MicroMount™ using Paratone® N (Hampton Research). The data integration and reduction were performed using the APEX3 v2019.1-0 (Bruker AXS, 2019) software suite. The integrations of the reflections were performed with SAINT 8.40A and the intensities collected were corrected for Lorentz and polarization effects and for absorption by semi-empirical

methods based on symmetry-equivalent data using SADABS 2016/2 of the suite software. The structures were solved by the dual-space algorithm implemented in SHELXT2014/5 program and were refined by least squares method on SHELXL2018/3.

Differential scanning calorimetry analysis

Variable pressure differential scanning calorimetry (VP-DSC) was performed at various applied pressures from 1 to 1000 bar using a Setaram μDSC7 EVO microcalorimeter. Samples of mass ~ 20 mg were tested in the temperature range of 315 – 370 K, using a 1.2 K min^{-1} heating/cooling rate.

Calculation of the volumetric entropy change

We have calculated the volumetric entropy change related to the bulk modulus of the material according to the methods reported in A. Aznar, *et al.*, *Appl. Mater. Today*, 2021, **23**, 101023:

$$\Delta S_V = \alpha B_o \cdot \Delta V_{tr} \quad \text{(Eq. 1)}$$

where α, B_o, and ΔV_{tr} denote volumetric thermal expansion coefficient, bulk modulus, and the specific volume change of the phase transition temperature, respectively. The obtained value of ΔS_V is approximately ~31 J K^{-1} kg^{-1}.

Additional figures

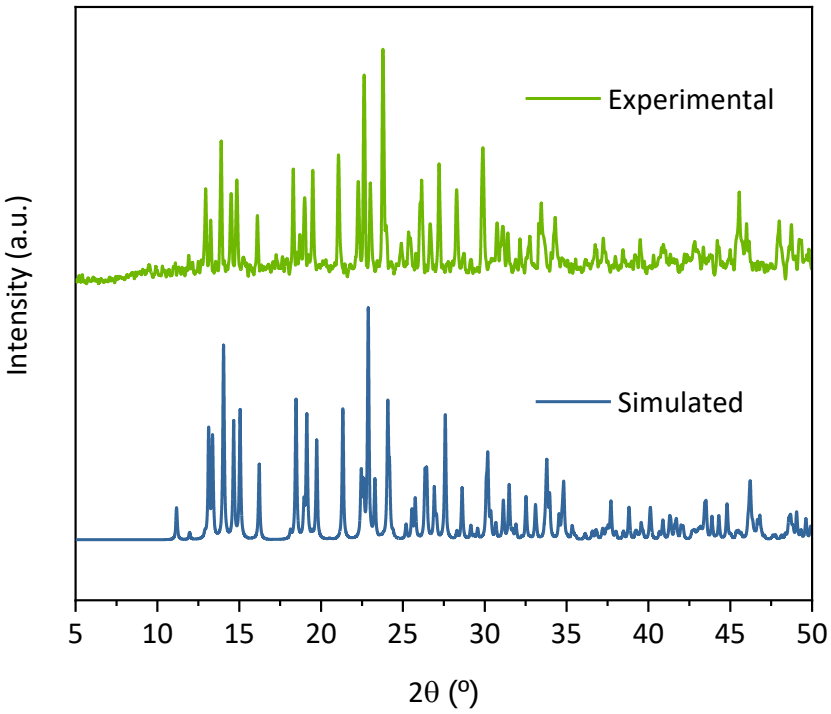

Figure S1. Room temperature experimental PXRD pattern of the $[(CH_3)_3NOH]_2[CoCl_4]$ compound compared with the simulated pattern obtained using the obtained crystal structure by single crystal XRD experiments.

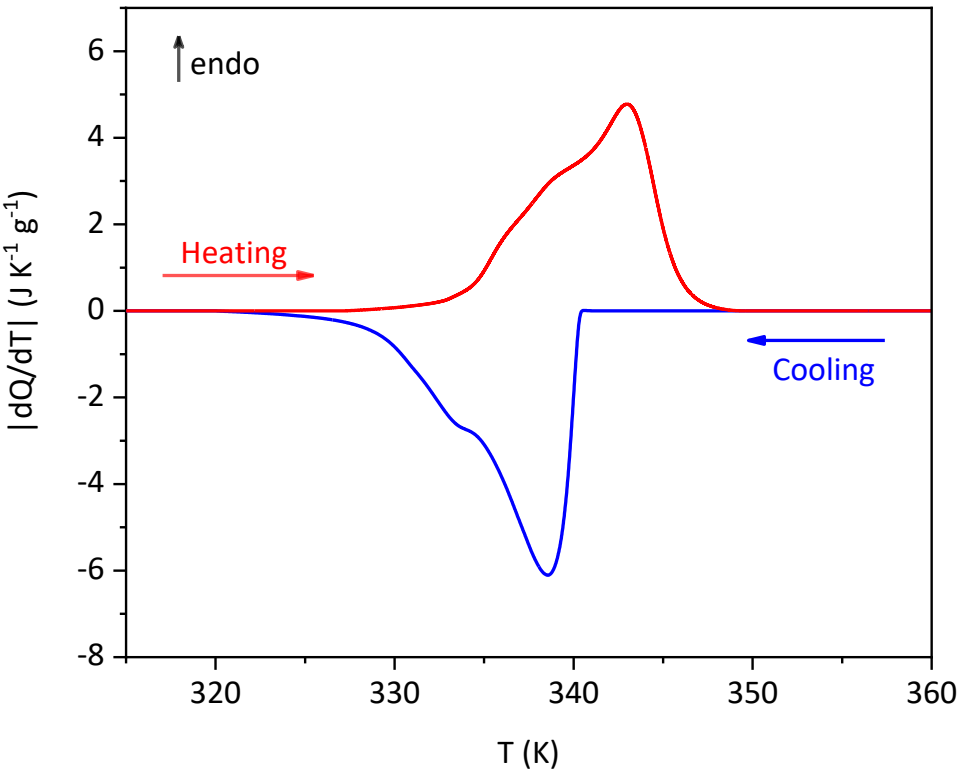

Figure S2. DSC curves for the $[(CH_3)_3NOH]_2[CoCl_4]$ compound at atmospheric pressure.

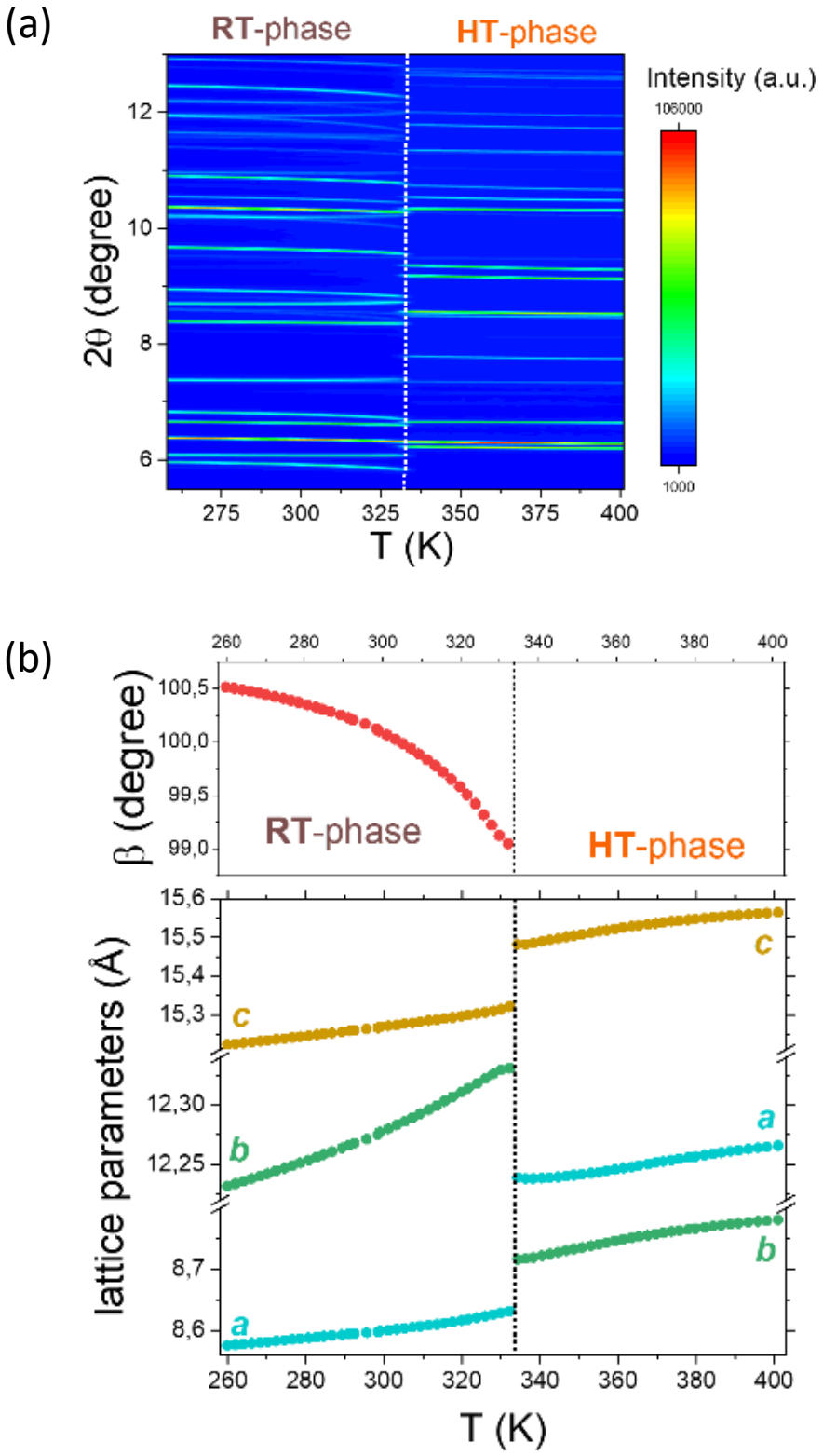

Figure S3. (a) Contour plot of SPXRD patterns at different temperatures and at atmospheric pressure. Evolution of (b) the lattice parameters of $[(CH_3)_3NOH]_2[CoCl_4]$ as a function of temperature.

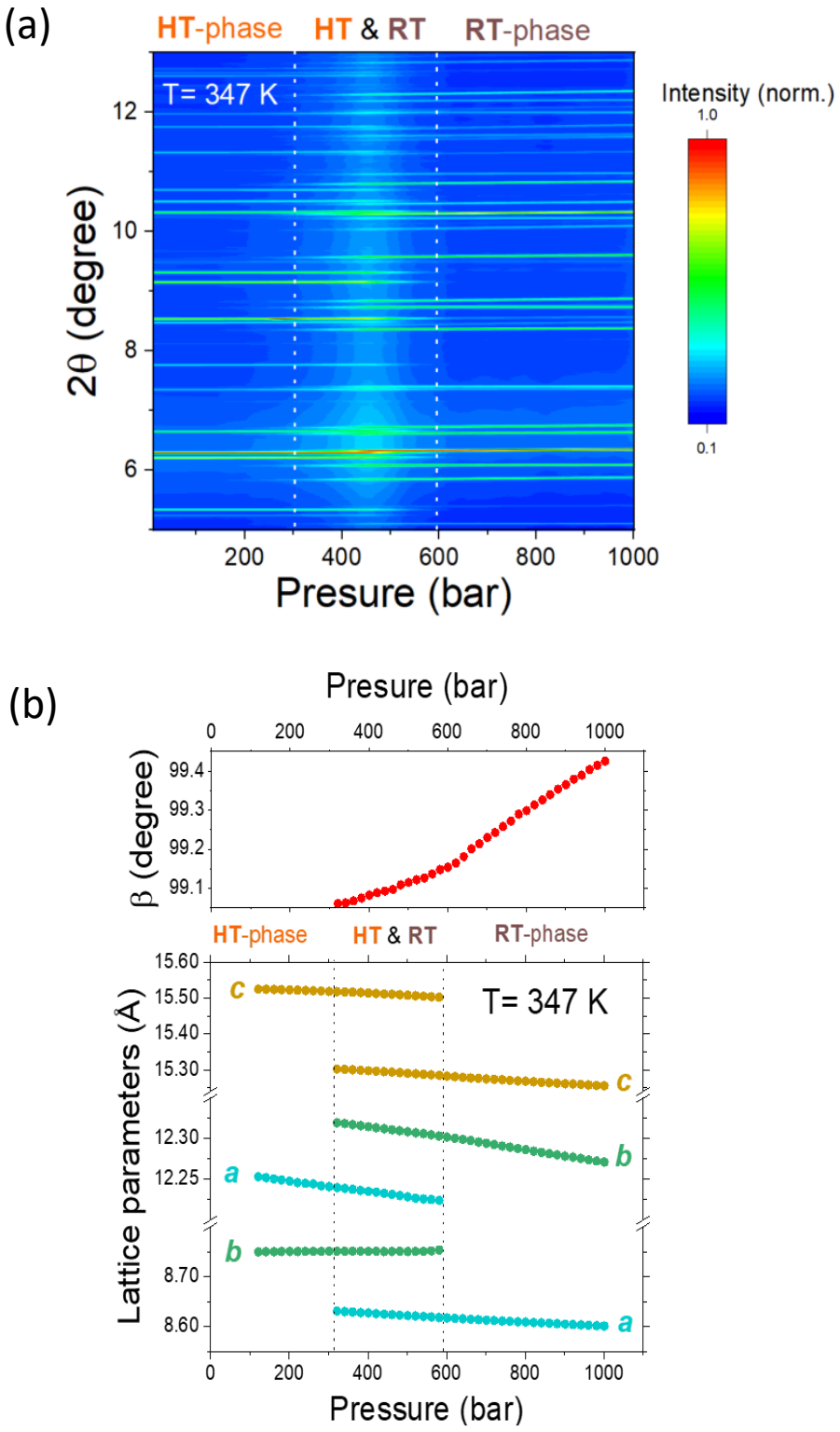

Figure S4. Contour plot of SPXRD patterns at different pressure under at isothermal conditions *T* = 347 K (a). Evolution of the lattice parameters and beta angle as a function of pressure at *T* = 347 K (b).

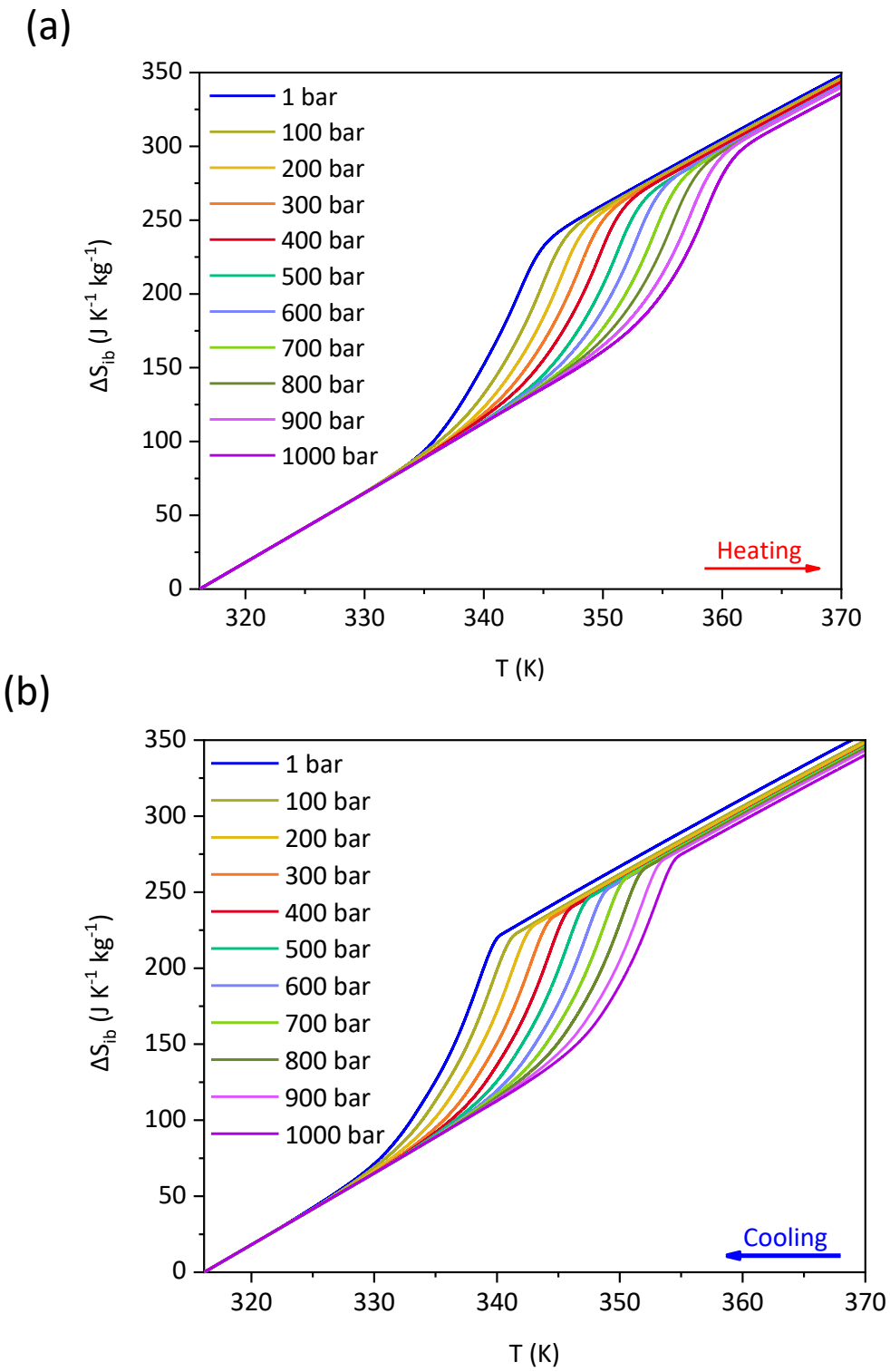

Figure S5. Obtained ΔS_{ib} *versus* temperature at different applied pressures on (a) heating and (b) cooling.

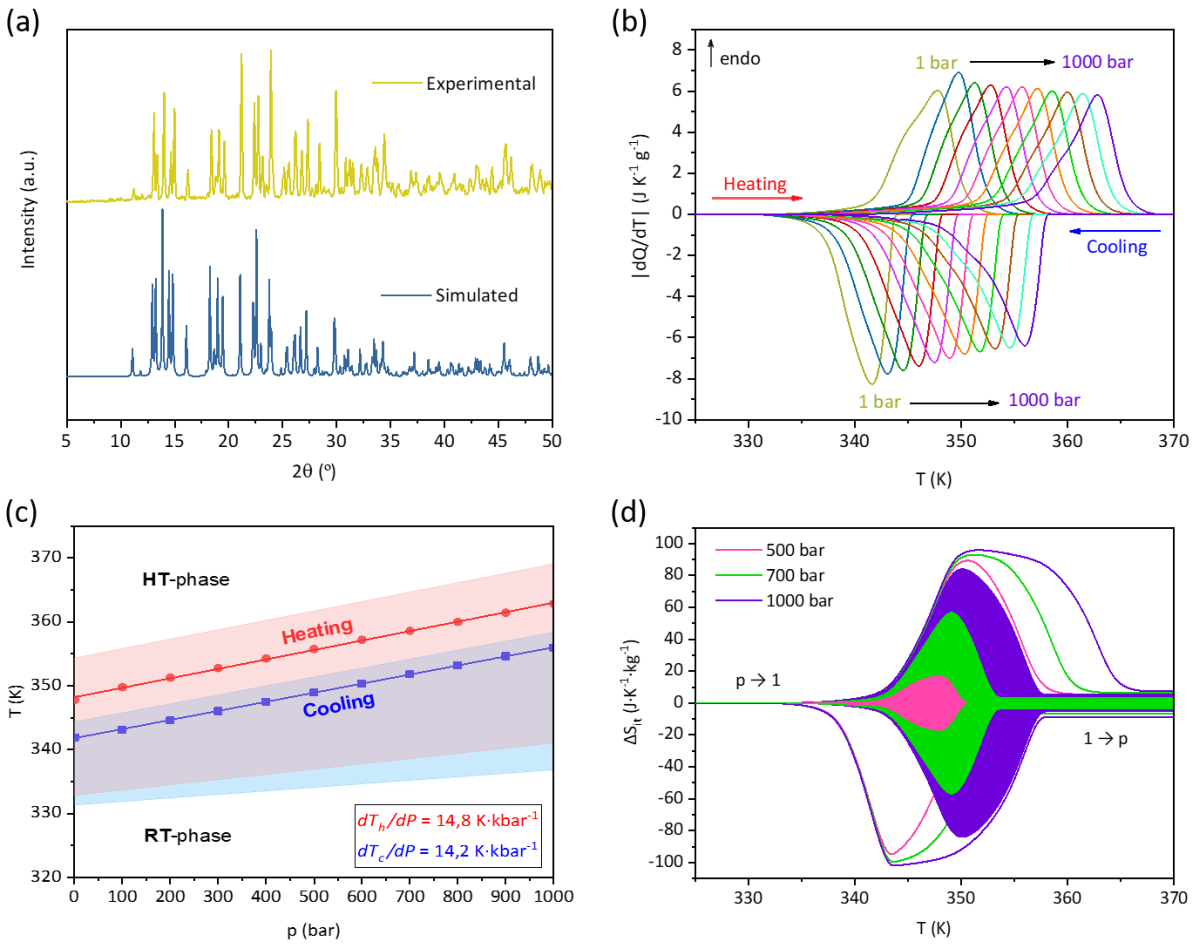

Figure S6. (a) Room temperature experimental PXRD pattern of the $[(CH_3)_3NOH]_2[CoCl_4]$ compound compared with the simulated pattern obtained using the obtained crystal structure by single crystal XRD experiments. (b-d) Barocaloric analysis for the $[(CH_3)_3NOH]_2[ZnCl_4]$ compounds following the similar procedure than for the Co-compound. (b) IdQ/dTI versus T curves at different isobaric conditions from 1 bar to 1000 bar in steps of 100 bar. The different peaks represent the heat flow associated to the phase transition. (c) T-p phase diagram built with the peaks maximum observed by DSC on heating (red curve) and cooling (blue curve). (d) Barocaloric effects in term of isothermal entropy change ΔS_{it} (coloured lines) and the reversible region ΔS_{rev} (shaded areas) as obtained by quasi-direct methods.

Table S1. Crystallographic data and structure refinement for $[(CH_3)_3NOH]_2CoCl_4$ at 100 K and 355 K.

	$[(CH_3)_3NOH]_2CoCl_4$ - RT phase	$[(CH_3)_3NOH]_2CoCl_4$ – HT phase
CCDC number	2387156	2387157
Empirical formula	$C_6H_{20}Cl_4CoN_2O_2$	$C_6Cl_4CoN_2O_2$
Formula weight	352.97	332.81
Temperature	100 K	355 K
Crystal system	Monoclinic	Orthorhombic
Space group	$P2_1/n$	*Pnma*
a	8.4749(6) Å	12.2008(6) Å
b	12.0762(8) Å	8.7001(4) Å
c	15.0400(10) Å	15.4434(8) Å
α	90°	90°
β	100.772(2)°	90°
γ	90°	90°
Volume	1512.14(18) $Å^3$	1639.29(14) $Å^3$
Z	4	4
ρ_{calc}	1.550 g/cm^3	1.348 g/cm^3
μ	1.827 mm^{-1}	1.682 mm^{-1}
F(000)	724.0	644.0
Crystal size	0.205 × 0.153 × 0.152 mm^3	0.205 × 0.153 × 0.152 mm^3
Radiation	MoKα (λ = 0.71073)	MoKα (λ = 0.71073)
2Θ range for data collection	4.356 to 72.682°	4.254 to 43.93°
Index ranges	$-14 \le h \le 13$ $0 \le k \le 20$ $0 \le l \le 25$	$-12 \le h \le 12$ $-9 \le k \le 9$ $-16 \le l \le 16$
Reflections collected	7335	25578
Independent reflections	7335 [R_{int} = 0.0593, R_{sigma} = 0.0268]	1071 [R_{int} = 0.0359, R_{sigma} = 0.0128]
Data / restraints / parameters	7335 / 0 / 144	1071 / 0 / 96
Goodness-of-fit on F^2	1.111	1.512
Final R indexes [I>=2σ (I)]	R_1 = 0.0286 wR_2 = 0.0586	R_1 = 0.0946 wR_2 = 0.3111
Final R indexes (all data)	R_1 = 0.0382 wR_2 = 0.0611	R_1 = 0.1065 wR_2 = 0.3417
Largest diff. peak/hole	0.41/-0.59 e $Å^{-3}$	0.43/-0.58 e $Å^{-3}$

Table S2. Selected bond distances (Å) for $[(CH_3)_3NOH]_2CoCl_4$ at 100 K and 355 K.

	100 K	**355 K**
Co-Cl		
Co(01)-Cl(1)	2.3064(3)	2.240(4)
Co(01)-Cl(2)	2.2964(3)	2.221(3)
Co(01)-Cl(3)	2.2415(3)	2.221(3)
Co(01)-Cl(4)	2.2578(3)	2.258(4)
O-N		
O(2)-N(2)	1.4262(10)	
O(1)-N(1)	1.4258(11)	
N-C		
N(2)-C(5)	1.4904(12)	
N(2)-C(5)	1.4933(12)	
N(2)-C(6)	1.4946(13)	
N(1)-C(2)	1.4882(13)	
N(1)-C(1)	1.4900(13)	
N(1)-C(3)	1.4898(14)	

Table S3. Selected bond angles (°) for $[(CH_3)_3NOH]_2CoCl_4$ at 100 K and 355 K.

	100 K	**355 K**
Cl-Co-Cl		
Cl(2)-Co(01)-Cl(1)	107.403(9)	112.0(2)
Cl(3)-Co(01)-Cl(1)	110.740(11)	109.08(14)
Cl(3)-Co(01)-Cl(2)	109.645(11)	109.08(14)
Cl(3)-Co(01)-Cl(4)	112.366(12)	108.4(2)
Cl(4)-Co(01)-Cl(1)	107.396(10)	109.14(15)
Cl(4)-Co(01)-Cl(2)	109.140(12)	109.14(15)
O-N(2)-C		
O(2)-N(2)-C(5)	108.99(7)	
O(2)-N(2)-C(4)	104.50(7)	
O(2)-N(2)-C(6)	109.63(7)	
C-N(2)-C		
C(5)-N(2)-C(4)	111.21(8)	
C(5)-N(2)-C(6)	111.27(8)	
C(4)-N(2)-C(6)	111.01(8)	
O-N(1)-C		
O(1)-N(1)-C(2)	108.93(8)	
O(1)-N(1)-C(1)	109.24(8)	
O(1)-N(1)-C(3)	104.18(8)	
C-N(1)-C		
C(2)-N(1)-C(1)	111.51(8)	
C(3)-N(1)-C(2)	111.29(9)	
C(3)-N(1)-C(1)	111.40(9)	

Table S4. Principal coefficients of thermal expansion and corresponding principal axes determined for $[(CH_3)_3NOH]_2CoCl_4$ at different temperature ranges: a) 260 <*T* (K)< 290 K and b) 290 <*T* (K)< 330 K. The thermal expansion (TE) along the principal axes were determinate using the web-based tool PASCal v2 (a web tool for Principal Axis Strain Calculations; https://www.pascalapp.co.uk).

a)

260 <*T* (K)< 290 K	
α (MK-1)	**Direction**
4(1)	$[\bar{1}01]$
91(1)	[010]
170(4)	[102]

b)

290 <*T* (K)< 330 K	
α (MK-1)	**Direction**
-113 (7)	$[\bar{1}01]$
135(2)	[010]
406(17)	[102]

Table S5. Comparison of barocaloric parameters between the $[(CH_3)_3NOH]_2[CoCl_4]$ and the $[(CH_3)_3NOH]_2[ZnCl_4]$.

Compound	T_h (K)	T_c (K)	ΔH (J g^{-1})	dT_t/dp (K $kbar^{-1}$)	ΔS_{rev} at 1000 bar (J K^{-1} Kg^{-1})
$[(CH_3)_3NOH]_2[CoCl_4]$	343	338	36	15.3	94
$[(CH_3)_3NOH]_2[ZnCl_4]$	348	342	35	14.5	84